Aging of Precipitated Amorphous Alumina Gel

J. M. Rousseaux,*,† P. Weisbecker,‡ H. Muhr,§ and E. Plasari§

Laboratoire des Sciences du Génie Chimique-CNRS, Ecole Nationale Supérieure des Industries Chimiques-INPL, 1 rue Grandville, B.P. 451, 54001 Nancy Cedex, France, Aluminium Pechiney, R & D Alumine B.P. 54, 13 541 Gardanne Cedex, France, and Laboratoire de Sciences et Génie des Matériaux Mêtalliques-CNRS, Ecole des Mines de Nancy-INPL, Parc de Saurupt, 54042 Nancy Cedex, France

Freshly precipitated alumina gel consists of very small particles (amorphous to XRD) that are agglomerated into larger particles (∼12 μm). When those particles are abruptly transferred into a solution at a pH equal or greater than 7 and at a temperature greater than 65 °C, an aging process occurs. The experiments performed in this work indicate that there are two mechanisms in the aging process, structural rearrangement and Ostwald ripening. The two mechanisms occur simultaneously, but their kinetics are very different. In the first period (i.e., the first 5 min of aging), the structural rearrangement mechanism is very rapid and governs the aging of the alumina (the particles undergo a dramatic water loss), whereas in the second period, the structural rearrangement is almost finished, and Ostwald ripening controls the aging process. The influence of the aging conditions (temperature, pH, and salt solution concentration) on the particle size distribution, crystallite size, crystallinity, specific surface area, total pore volume, and total water content is investigated, and the mechanisms of ripening are elucidated. The kinetics of Ostwald ripening are well quantified by a semiempirical equation that can be used for practical purposes.

Introduction

In addition to crystalline forms, aluminum hydroxide also occurs in amorphous and gelatinous forms. The compositions and properties of aluminum hydroxide gels, which are of considerable technical and commercial importance, largely depend on the method of preparation.[1] The solubility of aluminum hydroxide is very low in the pH range of 4−8. Aluminum hydroxide readily dissolves in strong acids and bases. Because of the steep slopes of the solubility curve, a slight variation in pH toward a value in the range of 4−9 can cause considerable supersaturation and, consequently, rapid and voluminous precipitation of aluminum hydroxide. As a result, the precipitate is generally of colloidal size and low crystalline order. Being hydrophilic, the fine precipitate readily forms gels.

Aluminum hydroxide gels formed by neutralization from either acid or basic solution contain considerable excesses of water and variable amounts of ions. Even after prolonged drying at 100−110 °C, the water contents of such gels can be as high as 5 mol of H_2O per mole of Al_2O_3.[2] Several factors determine the properties (water content, crystallite size, specific surface area, etc.) of gelatinous aluminas: temperature, final pH value, ionic composition, concentrations of initial solutions, and time of aging.

Because of their technical importance, the preparation and properties of the so-called alumina gels have been widely studied. An extensive review is given by Wefers and Misra.[2] They conclude that the various methods of preparation lead to three types of gelatinous products. The predominant solid phases in these gels can be (1) X-ray-indifferent (amorphous); (2) gelatinous boehmite, also termed pseudo-boehmite; or (3) finely crystallized trihydroxide (e.g., bayerite, nordstrandite, or gibbsite). Pseudo-boehmite is regarded as a poorly crystallized oxyhydroxide similar to boehmite, with a water content of 1.5−2.5 mol of H_2O per mole of Al_2O_3.[3] The XRD pattern of pseudo-boehmite shows broad lines that coincide with those of boehmite.[2]

Except for materials prepared at pH's above 7 and elevated temperatures, the initial product is always X-ray-indifferent. Depending on the operating conditions, transformation to crystalline hydroxide (aging) can occur. The first X-ray crystalline phase in the aging sequence is similar to that of boehmite and is called gelatinous or pseudo-boehmite.

It is obviously desirable for aging conditions to be optimized so that they provide a complete transformation to the appropriate crystalline phase and particle properties in the minimum time. To determine such conditions, all factors controlling the aging process should be identified and quantified. Various studies have shown the transformation of amorphous alumina gels into pseudo-boehmite to be highly dependent on the aging environment.[4−6] These reports emphasize mainly the morphology and properties of the product, such as the particle size, surface area, composition, and dehydration behavior, but the detailed conditions and the mechanism of product formation have never been well understood, nor have the transformation rates been quantified.

In most cases, the alumina precipitates are produced in the aqueous phase through the reaction between an aluminum salt (sulfate or chloride) and sodium hydroxide or sodium aluminate in different types of reactors in batch or continuous regimes. From this reaction, many valuable products with very different end-use properties can be obtained depending on process installation and operating conditions. Thus, the aim of this

* To whom correspondence should be addressed.
† Aluminium Pechiney.
‡ Ecole des Mines de Nancy-INPL.
§ Ecole Nationale Supérieure des Industries Chimiques-INPL.

10.1021/ie000053p CCC: $22.00
Published on Web 10/31/2002

study is to investigate and understand the influence of factors such as the time, temperature, pH, and salt solution concentration on the nature of the final product and also to determine the rate at which the phase transformation occurs. The investigation is focused on situations largely encountered in industry for obtaining widely varying products ranging from anti-gastric pharmaceuticals to catalysts and catalyst supports.

Theory

Aging is a process by which the physical properties of a solid phase can change as a result of the following mechanisms:[7] (a) recrystallization of the primary particles (e.g., needles, dendrites, thin plates, etc.) into more compact shapes through surface diffusion or mass transport through the liquid phase; (b) transformation of metastable crystal modifications into stable modifications by dissolution and recrystallization; (c) aggregation of primary particles and subsequent intergrowth; and (d) growth of larger particles at the expense of smaller ones (Ostwald ripening). As this is a rather broad complex of processes with poorly known mechanisms, no general theory has been developed to describe aging as a whole.

Aging is most important for poorly soluble substances. A typical aging process is a slow transformation of the precipitated amorphous phase into a crystalline modification. Chemical changes during aging appear, for instance, in metal hydroxide precipitates, where the nonstructural (adsorbed or located interstitially in the lattice) and structural (chemically bonded to the metal) water contents are decreased. A large amount of nonstructural water is contained in freshly precipitated hydroxides and is released during aging as a result of lattice reorganization and the growth of crystalline particles. For example, $Mg(OH)_2$ and $Cr(OH)_3$ particles follow this kind of aging process.[7]

The particle size distribution of a precipitate kept in contact with its mother liquor can change as a result of the dependence of the equilibrium solubility on the particle size, as described by the Gibbs−Thomson relation

$$\ln\left[\frac{a(r)}{a_{eq}}\right] = \frac{2\phi_s}{3\phi_v}\frac{\sigma V_m}{RT}\frac{1}{r} \tag{1}$$

where r is a characteristic dimension of the crystal and a is the activity of the solute defined by

$$a = \nu_+^{\nu_+}\nu_-^{\nu_-}\gamma_\pm^{\nu}c^{\nu} \tag{2}$$

Indeed, it follows from the Gibbs−Thompson relation (eq 1) that the activity of the substance in solution, and thus also the solubility of the solid particles, is a function of their size.

Because the solubility increases with decreasing crystal size, the solution can become undersaturated with respect to small crystals during the course of a batch precipitation while remaining supersaturated with respect to large crystals. Under these conditions, small crystals begin to dissolve, and the resulting solute is transported through the solution to the larger crystals, which continue to grow. The crystal size distribution of the precipitate thus shifts toward the larger sizes as time progresses. This process is generally called "Ostwald ripening". The rate of this aging process is determined by the size distribution of the precipitate, its growth kinetics, the mechanism controlling the crystal growth process, and the transport properties of the solution.

For diffusion-controlled growth, the maximum rate of ripening is given by Kahlweit[8] as

$$\frac{d\bar{r}^{\,3}}{dt} = \frac{8DV_m^{\,2}}{9}\frac{\sigma c_{eq}}{\nu RT} \tag{3}$$

Equation 3 also holds for growth controlled by a first-order surface reaction if D is substituted by k_1, the first-order rate constant. For a second-order surface reaction, the maximum rate of ripening is[8]

$$\frac{d\bar{r}^{\,3}}{dt} = \frac{16k_2V_m^{\,3}}{9}\left[\frac{\sigma c_{eq}}{\nu RT}\right]^2 \tag{4}$$

According to both eqs 3 and 4, the average crystallite size in a system undergoing Ostwald ripening is expected to follow a relation of the form

$$\frac{d\bar{r}^{\,3}}{dt} = A \tag{5}$$

where A is a rate constant defined in eqs 3 and 4.

The given equations do not permit predictions of the actual ripening rate, but only the maximum possible rate. As the initial assumptions in the derivations of eqs 3 and 4 are mostly not fulfilled, $d\bar{r}^3/dt$ and consequently the dependence of $\bar{r}$ on time can be considerably slower, i.e., up to several orders of magnitude.[7] A more general form of eq 5 has been used by Hanitzsch and Kahlweit[9] and Mullin et al.[10]

$$\frac{d\bar{r}^{\,n}}{dt} = B \tag{6}$$

where B is a rate constant and n is an exponent depending on the mechanism of ripening.

Gruy and Cournil[11] used eq 5 in modeling the aging of precipitates when mass diffusion is the rate-determining. In their case, the integrated form of eq 5

$$\bar{r}^{\,3} - \bar{r}_0^{\,3} = A(t - t_0) \tag{7}$$

where $\bar{r}_0$ is an initial mean characteristic crystal size at time t_0, agrees well with the experimental data. Similarly, integration of eq 6 leads to the equation

$$\bar{r}^{\,n} - \bar{r}_0^{\,n} = B(t - t_0) \tag{8}$$

It is interesting to write eqs 7 and 8 in the form

$$\bar{r} = \bar{r}_0\left[1 + \frac{A}{\bar{r}_0^{\,3}}(t - t_0)\right]^{1/3} \tag{9}$$

$$\bar{r} = \bar{r}_0\left[1 + \frac{B}{\bar{r}_0^{\,n}}(t - t_0)\right]^{1/n} \tag{10}$$

Equation 10 models the evolution of a mean characteristic crystal size of a solid particle as a function of time and three additional parameters: $\bar{r}_0$, B, and n. Equation 9 is a particular case of eq 10 in which $A = B$ and $n = 3$. In this work, a nonlinear regression is used to

determine the three parameters of eq 10 from the experimental data.

Experimental Section

Reagents. Amorphous alumina gel was obtained by mixing aqueous solutions of $NaAl(OH)_4$ and $Al_2(SO_4)_3$ at pH 4 and at a temperature of 25 °C. The initial sodium aluminate solution typically included a caustic concentration of 280.7 g L^{-1} (as Na_2O) and an alumina concentration of 319 g L^{-1} (as Al_2O_3), giving a Na_2O/Al_2O_3 molar ratio of 1.44. The initial aluminum sulfate solution contained sulfates at a concentration of 298.4 g L^{-1} and alumina at a concentration of 112 g L^{-1} (as Al_2O_3). Adequate dilution of the initial reagents was doneto generate precipitate suspensions of the desired alumina concentration.

Precipitation. The amorphous alumina gel was precipitated in a continuous stirred tank reactor comprising a 2.5-L stainless steel flat-bottomed vessel characterized by a standard configuration, namely, $H = T_v$, $D_R = T_v/3$, and $h = H/3$ (where T_v is the diameter of the vessel, which is equal to 0.15 m; D_R is the diameter of the Rushton turbine; H is the height of the liquid in the vessel; and h is the clearance between the stirrer and the bottom of the reactor). Four wall baffles of width $T_v/10$ prevent vortexing. In addition, the reactor is flat-bottomed, jacketed and maintained at 25 °C by a thermostatic bath. The sodium aluminate and aluminum sulfate solutions were introduced continuously in the discharge flow of the Rushton turbine having a stirring speed of 600 rpm, corresponding to a mean power consumption of $\bar{\epsilon} = 0.7$ W kg^{-1}. The pH os 4.0 (measured in the bulk of the precipitator) was controlled by manual adjustment of the ratio of the pumping speeds of two peristaltic pumps. A residence time of 10 min was used for the precipitation process in all experiments. After steady state had been attained (i.e., after a period 8 times the length of the residence time), alumina gel suspension was recovered at the outlet of the precipitator. Two different reactant solutions were used to give amorphous alumina gel concentrations of 60 and 120 g L^{-1} after reaction.

Sampling Procedure. Gelatinous aluminas prepared by the neutralization of concentrated aluminum salt solutions at temperatures below 290 K have low crystalline order and very small particle sizes. The rate of aging (i.e., transformation of the amorphous solid phase into ordered aluminum hydroxide) is also very slow at these temperatures.[2] Consequently, the samples taken during aging were immediately quenched in cold deionized water before being washed and filtered. Exactly the same quenching, washing, and filtering procedures were adopted for all samples.

Aging Experiments. Aging experiments were carried out in the same standard-configuration 2.5-L jacketed vessel maintained at the desired aging temperature (65, 75, or 85 °C). The Rushton turbine was rotated at 600 rpm for all aging experiments. To complete the data, one experiment was carried out at 1200 rpm, corresponding to a mean power consumption of $\bar{\epsilon} = 5.5$ W kg^{-1}. Two alumina particle suspension concentrations were investigated: 20 and 50 g L^{-1}. The amorphous alumina gel suspensions were instantaneously introduced into sodium hydroxide solutions of fixed pH. Thus, the alumina particle suspension with the concentration of 20 g L^{-1} was prepared by introducing instantaneously 830 mL of 60 g L^{-1} initial amorphous alumina gel suspension into 1670 mL of sodium hydroxide solution. Similarly, 1040 mL of 120 g L^{-1} initial amorphous alumina gel solution and 1460 mL of sodium hydroxide solution were mixed to give the alumina particle suspension concentration of 50 g L^{-1}. The sodium sulfate (Na_2SO_4) concentrations of the thus-prepared alumina particle suspensions of concentrations 20 and 50 g L^{-1} were 23 and 57 g L^{-1}, respectively.

Techniques. Washing, filtering, and drying were accomplished by sampling 30 mL of suspension and introducing it instantaneously into 250 mL of filtered and deionized cold tap water. The resulting suspension was then immediately filtered using a classical vacuum filtration setup. The membrane filters used were supported 0.22-μm AcetatePlus filters from MSI. All samples were vacuum-dried at 40 °C for 72 h. No structural changes were observed during the treatment of samples; for example, the initial amorphous alumina remained amorphous after the described treatment.

Particle size distributions were determined using a Malvern Mastersizer S laser diffraction granulometer. With this instrument, the size of the agglomerates corresponds to the diameter of a circle formed by the projection of the rotating agglomerate on the plane of the detectors. In the case of amorphous alumina particles, the suspension was sampled at the outlet of the reactor, whereas during aging, the representative suspension was sampled from the bulk of the aging vessel.

For nitrogen-gas-adsorption measurements, dried particle samples obtained after sampling and subsequent filtering, washing, and drying were outgassed at room temperature with nitrogen. Typical acquisition times were very long because outgassing of the alumina samples required at least 48 h and adsorption−desorption data acquisition generally took several hours. Adsorption isotherms were recorded at −196 °C with a Sorptomatic 1900 specific surface area analyzer (Carlo Erba Instruments). The surface area was determined by fitting the BET adsorption isotherm to the data points between relative pressures of 0.05 and 0.3 and using an area of 0.162 nm^2 per N_2 molecule. Measurements using three identical samples gave an error of 3%. The total pore volume V_p was calculated using the value $V_{0.98}$ of the total amount of N_2 molecules adsorbed obtained at the relative desorption pressure $P/P_0 = 0.98$. The total pore volume was then calculated according to the equation[12]

$$V_p = V_{0.98} \times \frac{28}{22\,414 \times 0.808} \tag{11}$$

In addition, t-plots were constructed to quantify the micropore volumes of the prepared aluminas. The Harkins−Jura equation

$$t = \sqrt{\frac{13.99}{0.034 - \log\left(\frac{P}{P_0}\right)}} \tag{12}$$

was used to calculate the statistical thickness of the adsorbate from the relative pressure ratio P/P_0.

For X-ray powder diffraction measurements, the radiation source was a monochromatic Co $K\alpha_1$ line (wavelength = 1.788 97 Å) originating from a conventional X-ray tube (Siemens Kristalloflex D500 in $\theta/2\theta$-type Bragg−Brentano mode primary monochromatic, linear detector) operated at 37.5 kV and 25 mA. Typical

acquisition times were 21 min for the 021 line only ($26.4° < 2\theta < 39.2°$) and 1 h 38 min for the entire spectrum ($20° < 2\theta < 150°$). The width of the 120 reflection of each pattern was measured at half-maximum intensity after subtraction of the background; the 2θ position of each 120 reflection was measured at the midpoint of the chord at half-maximum intensity. The 111 reflection of powdered silicon (the 111 peak is situated at 33.1°) was used as a standard for 2θ and as a measure of instrumental broadening. The width (b) of the 111 reflection of silicon was subtracted from the measured width of the 120 reflection (C) of boehmite to give the pure diffraction width (β), i.e., $\beta = C - b$. The well-known Scherrer equation was used to calculate the crystallite size (which is actually the mean crystallite dimension perpendicular to the 120 plane). The Scherrer equation is written as follows

$$\Lambda = \frac{0.9\lambda}{\beta \cos(\theta)} \tag{13}$$

As an example, for the 120 pseudo-boehmite peak situated at 32.4°, a width at half-maximum intensity of 2.79° and an instrumental broadening of 0.26° give a crystallite size of

$$\Lambda = \frac{0.9 \times 1.7889 \times 57.3}{2.53 \times \cos\left[\frac{32.4}{2 \times 57.3}\right]} = 38 \text{ Å} \tag{14}$$

The factor 57.3 was used to convert 2θ and β from degrees to radians.

The X-ray evaluation program software EVA, version 4.00, DIFFRAC Plus, from Bruker Analytical X-ray Systems was used to evaluate the diffraction widths. Measurements using three samples of the same material gave an error of 7%.

The apparatus used for the thermogravimetric analysis was a Setaram B70. The particles were heated at atmospheric pressure in the temperature range 110−1100 °C until a constant weight was obtained. A weight-loss profile was obtained by plotting the weight loss fraction (i.e., the total weight loss at a given temperature divided by the initial mass of the sample investigated) of these materials versus the heating temperature. In the present work, the pseudo-boehmite samples were heated in a helium atmosphere (725 Torr) at a rate of 20 °C min^{-1} to a maximum temperature of 1100 °C.

pH was measured with a Xérolyt Ingold Mettler Toledo electrode (resistant to high temperatures) using a Tacussel PHN330T pH meter.

Results

The evolution of particle properties (PSD, crystallite size, crystallinity, specific surface area, pore volume, and total water content) as a function of aging time is shown in Figures 1−10. Nonlinear regressions of eq 10 with experimentally obtained crystallite size values in Figures 2−4 indicate that the agreement between model and experiment for aging times from 0 to 5 min is poor, whereas, for aging times longer than 5 min ($t_o = 300$ s), the agreement is very good and gives an exponent value equal to $n = 3 \pm 0.1$ for all regressions. This observation means that the aging process involved here for running times longer than 5 min is Ostwald ripening (see eqs 5 and 9). For this reason, the regressions of the experimental results were repeated with the theoretical exponent $n = 3$, so eq 9 was used to correlate the experimental results and obtain values for the kinetic parameters $\bar{r}_0$ and A. Tables 1−3 give the regression parameters of eq 9.

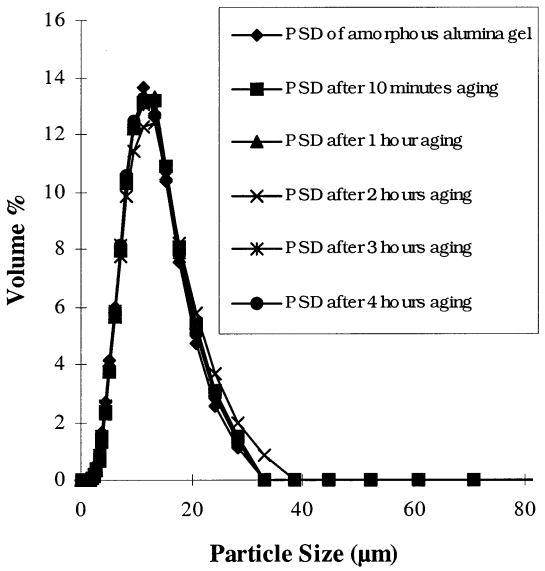

Figure 1. Volume-based particle size distribution at different aging times (initial alumina concentration = 20 g L^{-1}, pH = 11.0, and T = 65 °C).

Particle Size Distribution (PSD). In all cases, the alumina gels produced were composed of particles that represented agglomerates of elementary submicron particles. The size distributions of the particles (agglomerates) as a function of time are presented in Figure 1, where it is clearly shown that the volume-based (i.e., mass-based) distributions remained unchanged with aging time; no detectable change in agglomerate volume occurred during the aging process from the amorphous to the crystalline state, which is a very surprising result. The agglomerates were not destroyed and re-formed, so the phase transformation must be a phenomenon taking place in the interior of agglomerate particles. This conclusion is reinforced by the results of an experiment that gave essentially the same kinetic parameter values when the stirring speed was doubled.

Crystallite Size and Crystallinity. The aim of this section is to describe the influence of the aging conditions on the crystallite size and crystallinity of the elementary submicron alumina particles. The pseudo-boehmite structural order ranges from amorphous (i.e., X-ray-indifferent) to crystalline. X-ray-indifferent structures indicate a lack of sufficient long-range order to produce a diffraction pattern with X-rays in the 0.1−0.2-nm wavelength range. Thus, pseudo-boehmite is a poorly crystallized alumina with an X-ray diffraction pattern similar to that of boehmite. It differs from boehmite in several aspects. Its lower degree of crystallinity is reflected in the broader X-ray diffraction lines, especially the 020 line (b crystallographic dimension), which increases from about 6.1 Å in well-crystallized boehmite to as much as 6.6−6.7 Å in pseudo-boehmite.[5]

X-ray diffraction patterns of pseudo-boehmite contain very broadened diffraction lines. The size of the boehmite crystallites was determined in this work from the broadening of the 021 reflection using the well-known Scherrer equation. The half-width of an XRD peak is the result of defects in the crystalline structure as well as crystallite size, so the measurement is useful for the

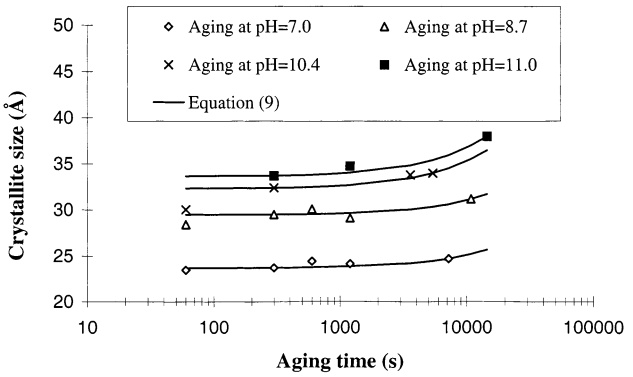

Figure 2. Crystallite size as a function of aging time for several solution pH values (T = 75 °C and initial alumina concentration = 20 g L^{-1}).

Table 1. Constants of Eq 9 Expressing Pseudo-Boehmite Aging Rates for the Results Presented in Figure 2

pH	$\bar{r}_0$ (Å)	A (Å^3 s^{-1})
7.0	23.6	0.28
8.7	29.4	0.48
10.4	32.3	1.43
11.0	33.6	1.99

relative value of the size.[13] X-ray measurements give relative values that depend on the peak in the pattern. Johnson and Mooi[14] arbitrarily selected the 310 plane to determine pseudo-boehmite crystallite sizes. Ono and Oghuchi[15] characterized pseudo-boehmite crystallite sizes correponding to the 020 plane, whereas Misra[1] compared crystallite sizes calculated using the 020 and 021 planes of commercial pseudo-boehmite recovered at the outlet of a plant precipitator. He reported that the crystallite size calculated using the 020 reflection is approximately 65% of the value of the crystallite size calculated using the 021 reflection.

In the present work, the investigated aging conditions are the pH, temperature, and salt concentration of the solution. Figure 2 represents the experimental and model-predicted (eq 9) variations of the crystallite size as a function of time for initially amorphous alumina particles aged at four different pH values. The kinetic parameters obtained by fitting are reported in Table 1. From Figure 2, it appears that model eq 9 agrees well with the experimental data and that the increase of the crystallite size as a function of aging time is very slow. In addition, for a given aging time, the crystallite size increases with increasing pH. The parameter A is proportional to the volume growth rate of the crystallites. Table 1 shows a significant increase in growth rate (by a factor of 8) as the pH increases from 7.0 to 11.0. In particular, the increase in the volume growth rate is very sharp in the pH range from 8.7 to 10.4. In addition, Figure 3 and Table 2 clearly show the strong influence of the temperature on the aging rate. For approximately the same pH value, the volumetric growth rate constant A increases significantly as the temperature increases.

When alumina is precipitated, an equivalent quantity of sodium sulfate is produced. Thus, the solution is charged with sodium and sulfate ions, which might influence the kinetic parameters of the aging process. In accordance with industrial conditions, two alumina suspension concentrations (20 and 50 g L^{-1}) and corresponding concentrations of sodium sulfate (23 and 57 g L^{-1}) were investigated. Figure 4 displays the crystallite size as a function of time for initially amorphous alumina particles of two different salt concentrations,

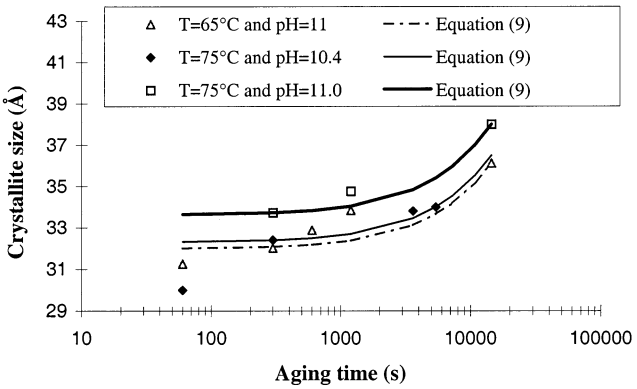

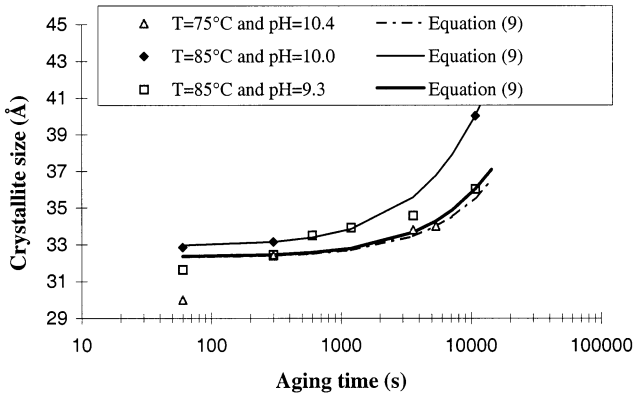

Figure 3. Crystallite size as a function of aging time for three temperatures and two pH values (initial alumina suspension concentration = 20 g L^{-1}).

Table 2. Constants of Eq 9 Expressing Pseudo-Boehmite Aging Rate for the Results Presented in Figure 3

pH	T (°C)	$\bar{r}_0$ (Å)	A (Å^3 s^{-1})
11.0	65	32.0	1.00
10.4	75	32.3	1.43
11.0	75	33.6	1.99
9.3	85	32.3	1.23
10.0	85	32.9	2.59

Table 3. Constants of Eq 10 Expressing Pseudo-Boehmite Aging Rate for the Results Presented in Figure 4

pH	C_{AS} (g L^{-1})	$\bar{r}_0$ (Å)	A (Å^3 s^{-1})
7.0	20	23.6	0.28
7.0	50	24.6	1.14
10.4	20	32.3	1.69
10.0	50	26.9	2.08

and the parameter values optimized by fitting the results are given in Table 3, showing that, as the salt solution concentration increases from 20 to 50 g L^{-1}, the rate constant A of eq 9 increases significantly.

Figure 5 presents an XRD pattern of initially amorphous alumina gel aged for 4 h. Noteworthy is that the XRD pattern shows broad lines that coincide with those of boehmite, which is characteristic of pseudo-boehmite particles. In addition, the aging process led to pure pseudo-boehmite particles; no trace of other polymorphs (bayerite, gibbsite, nordstrandite, etc.) was observed.

Figure 6 shows that the aging of initially amorphous alumina gel very rapidly (actually within the first minute) gives rise to the broadened XRD patterns of boehmite that are characteristic of pseudo-boehmite.

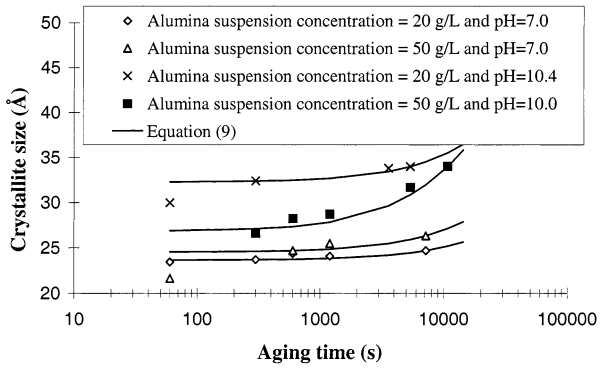

Figure 4. Crystallite size as a function of aging time for two alumina suspension concentrations and two pH values (T = 75 °C).

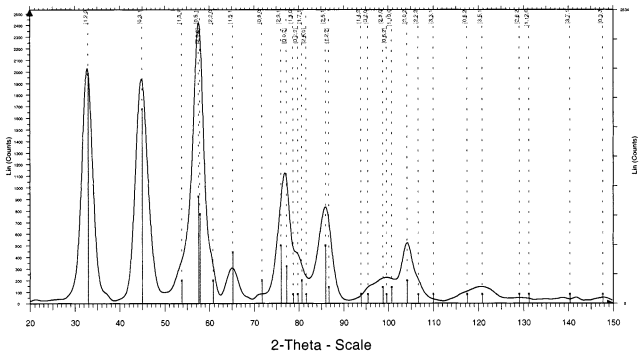

Figure 5. X-ray diffraction pattern of initially amorphous alumina gel aged for 4 h in a solution having pH = 11.0 and T = 75 °C.

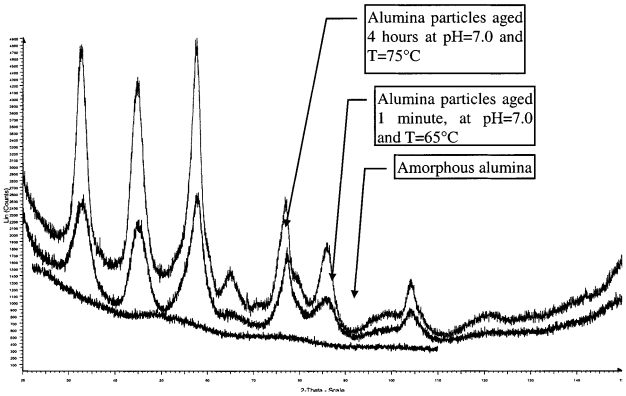

Figure 6. X-ray diffraction patterns of alumina particles aged from initially amorphous alumina gel.

The term pseudo-boehmite refers to only those aggregates that are large enough to precipitate from solution, including X-ray-amorphous gels, as well as those materials that give rise to broadened XRD patterns of boehmite.[16] However, it should be possible to prepare an amorphous gel having the atomic ordering characteristics of gibbsite and bayerite. Nevertheless, according to the opinion of Baker and Pearson,[16] gels that do not age into these phases do not contain bayerite or gibbsite ordering. Thus, it can be concluded from Figure 6 that the initially amorphous alumina gel contains pseudo-boehmite short-range ordering but has crystallite sizes that are too small to be detected by XRD. Little is known about the short-range structure of amorphous alumina structures.

Figure 7 shows the evolution of the 120 peak as a function of aging time for fixed aging conditions. It

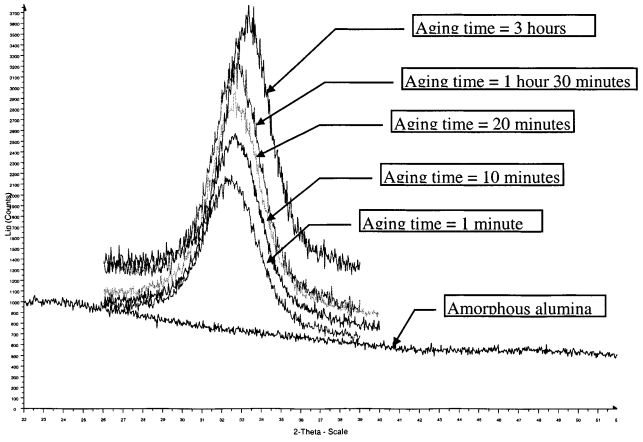

Figure 7. Example of successive X-ray diffraction peaks of initially amorphous alumina gel aged in the solution having pH = 9.3 and T = 85 °C.

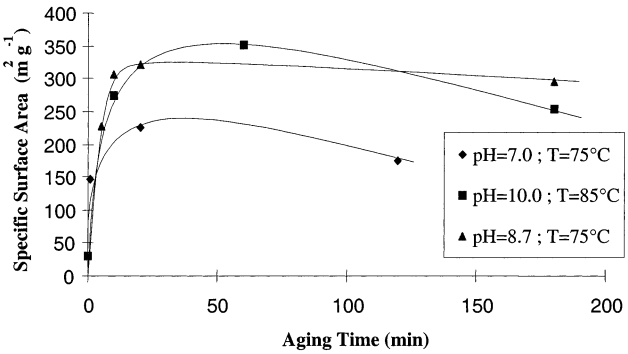

Figure 8. Specific surface area as a function of aging time (initial alumina concentration = 20 g L^{-1}).

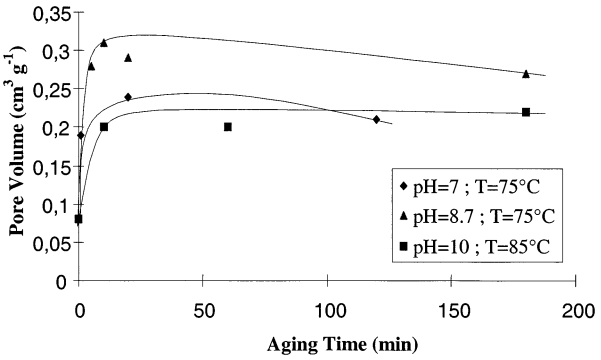

Figure 9. Pore volume as a function of aging time (initial alumina concentration = 20 g L^{-1}).

appears that the transition from the amorphous alumina line to a broad diffraction line occurs within the first minute of the aging process. Subsequently, as seen in Figure 7, the 120 peak shifts to the right while becoming narrower, which is likely due to the lattice contraction caused by intracrystalline water release.

Specific Surface Area and Porous Volume. Figure 8 shows the specific surface area as a function of aging time for three different aging conditions corresponding to initial alumina concentration of 20 g L^{-1}. The pore volume as a function of aging time is represented in Figure 9.

The initial amorphous alumina prepared in this work had a very low specific surface area of 30 m^2 g^{-1} and a very low total pore volume of 0.08 cm^3 g^{-1}. In addition, 11% of this pore volume was in the micropore volume region. During aging, even after only 1 min of aging

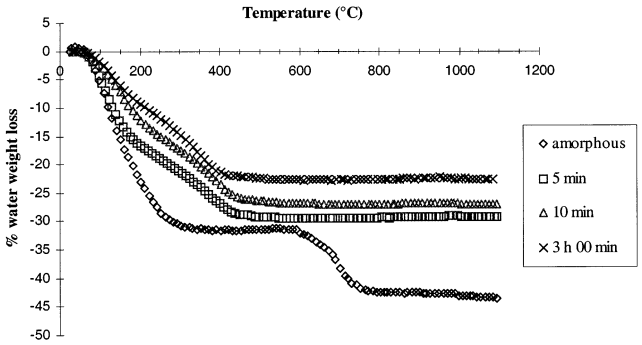

Figure 10. Weight-loss profile as a function of aging time (pH = 10.0, T = 85 °C, and initial alumina concentration = 20 g L^{-1}).

time, the micropore volume decreased rapidly to a maximum of 5 vol % and then continued to decrease to values lower than 1%. The total pore volume increased very rapidly to approximately 0.20 cm^3 g^{-1} and then remained almost constant.

A remarkable fact is that the specific surface area went through a maximum value that seems to have been situated between 10 and 50 min of aging time. This maximum value was approximately 230, 320, and 360 m^2 g^{-1} for alumina particles aged at pH values of 7, 8.7, and 10, respectively. After 50 min of aging, the specific surface area systematically decreased.

Thermogravimetric Data Analysis. It is very interesting to investigate the variation of water content and the forms of structural bonds of water in pseudo-boehmite during the aging process. The increase in the *b* crystallographic dimension is accompanied by an increase in the water content over the stoichiometric formula for boehmite, $Al_2O_3 \cdot 1H_2O$. Papée et al.[17] postulated that the excess water is not merely adsorbed on crystallite surfaces but, rather, is located between boehmite-like layers as molecular water, thus accounting for the increase in the *b* dimension of the crystallite.

Lippens[5] found as much as 30.7 wt % water in pseudo-boemite, instead of the 15 wt % that corresponds to the stoichiometric formula for boehmite, $Al_2O_3 \cdot 1H_2O$. He also observed a linear relationship between the increased *b* dimension and the mole fraction of excess water, concurring with Papée et al.,[17] who placed the excess water between the boehmite layers. Baker and Pearson[16] rejected Papée et al.'s and Lippens's intercalation model, ascribing all of the excess water to H_2O coordinated to Al on crystal surfaces. Wefers and Misra[2] reviewed the data for pseudo-boehmite and postulated a series of reactions leading to a structure similar to the previously proposed structures of Papée et al. and Lippens, i.e., $(AlOOH)_2 \cdots HOH \cdots (HOOAl)_2$. They state, rather clearly, that the excess water is not surface water, but interlayer water.

Data of Anderson cited by Baker and Pearson[16] show that, as the crystallite size becomes smaller, the water content increases abruptly, accompanied by a very large increase in the specific surface area. Pseudo-boehmite prepared in commercial processes or in the laboratory has crystallite sizes smaller than 50 Å and water contents of 20−30 wt %.

In the present work, the thermogravimetric data show a clear difference between the amorphous samples and the aged particles (see Figure 10). For the aged particles, the water weight loss decreases with aging time. The weight-loss profile for the amorphous particles is characterized by two plateaus. The first corresponds to the dehydration sequence of the initially amorphous particles into boehmite AlOOH (this transformation proceeds as the temperature increases from 110 to 400 °C), and the second corresponds to the dehydration of the obtained boehmite particles into Al_2O_3 particles (this transformation proceeds as the temperature increases from 580 to 800 °C). The sequence involved is as follows

$$\text{amorphous alumina} \xrightarrow{110\ ^\circ\text{C} < T < 400\ ^\circ\text{C}} \text{AlOOH} \xrightarrow{580\ ^\circ\text{C} < T < 800\ ^\circ\text{C}} Al_2O_3$$

The weight-loss value corresponding to the first plateau (p1) equals 31.5%, and the weight-loss value corresponding to the second plateau (p2) equals 42.0%. If m_{in} is the initial mass weight of the amorphous alumina sample, m_{p1} is the mass weight of the sample corresponding to its state at the first plateau, and m_{p2} is the mass weight of the sample corresponding to its state at the second plateau, one obtains

$$m_{p1} = m_{in}(1 - p1) \tag{15}$$

$$m_{p2} = m_{in}(1 - p2) \tag{16}$$

In our case

$$\frac{m_{p2}}{m_{p1}} = \frac{1 - p2}{1 - p1} \approx 0.85\ (85\%) \tag{17}$$

On the other hand, if we assume that the phase transformation from the first plateau to the second plateau (see Figure 10) corresponds to the reaction

$$2\text{AlOOH} \xrightarrow{580\ ^\circ\text{C} < T < 800\ ^\circ\text{C}} Al_2O_3$$

then the following molar mass ratio must be satisfied

$$\frac{M(Al_2O_3)}{2M(\text{AlOOH})} = \frac{102}{2 \times 60} = 0.85\ (85\%) \tag{18}$$

Thus, our assumption that AlOOH particles are present during the first plateau and Al_2O_3 particles during the second plateau is consistent.

From the X-ray diffraction analysis (see Figure 6), we know that the initially amorphous alumina particles are readily transformed (within the first minute) into pseudo-boehmite particles. The weight-loss profiles of these aged particles show three distinguishable regions.

It is known that pseudo-boehmite particles are a poorly crystallized boehmite with a high water content.[3] The adsorbed water is believed to exist in the forms of both "physisorbed" water and surface hydroxyl groups.[18] The first region of weight loss from 50 to 200 °C corresponds to a dehydration process that can be related to the removal of physisorbed and/or bulk molecular water prior to the condensation of the hydroxyl groups of the alumina material.

The second region is in the temperature range from 200 to 400 °C, which corresponds to dehydration through the condensation of Al−OH groups. The adjacent surface hydroxyls condense to form water molecules according to the dehydration reaction[18]

$$\sim\text{OH} + \sim\text{OH} \rightarrow \sim\text{O}\sim + \blacksquare + H_2O$$

where ■ represents an oxide vacancy for four- or five-coordinate AlO_x sites formed from six-coordinate sites.

Schematically, the following chemical process occurs

$$AlOOH \rightarrow AlO_{1+x} + OH_{1-2x} + xH_2O$$

At a temperature of approximately 400 °C, x attains a value of 0.5.

In the final region, which falls in the 400−1100 °C temperature range, no weight loss is observed. The Al_2O_3 particles, known to be refractory, remain stable in this temperature range.

The total water content of the initially amorphous alumina particles decreased continuously with time. After 5 min, 10 min, and 3 h of aging in a solution with a pH of 10, a temperature of 85 °C, and a particle concentration of 20 g L^{-1}, the total water contents of the obtained samples were equal to 29.2, 26.8, and 22.4%, respectively. This demonstrates that, during aging, the solid phase in the aqueous suspension loses a quantity of water when passing from alumina gel to pseudo-boehmite. The total water content of the initially amorphous alumina particles amounted to 42%. Consequently, a dramatic decrease of the total water content occurs during the first 10 min of the aging process. After this, the total water content continued to decrease with aging time but did so much more slowly.

Discussion

General Considerations. Ostwald ripening, i.e., the growth of larger crystals at the expense of smaller ones, is often cited as one of the prime causes of decreases in precipitate specific surface area during aging (resulting from a particle size increase). However, in this work, the specific surface area increased with aging time at the beginning of the aging process. For a system undergoing an aging process controlled by Ostwald ripening, the constant n in eq 6 is expected to have a value of 3. For aging times longer than 5 min, the values of n found in this work are all close to 3. Therefore, the conclusion is that, for times longer than 5 min, the aging of alumina gel is a process governed by the mechanism of Ostwald ripening that is well-characterized by eq 5. However, the specific surface area goes through a maximum (see Figure 8), which seems to indicate that there are two mechanisms in the aging process. The same observations are valid concerning the pore volumes (see Figure 9). The thermogravimetric data show that the particles undergo a loss of water as the aging process proceeds. During the first period (i.e., the first 5 min of aging), the particles undergo a dramatic water loss according to a structural rearrangement mechanism from an amorphous to a crystalline product, as shown by XRD (see Figures 6 and 7). In the second period, the particles continue to lose water steadily but much more slowly. Generally speaking, the two mechanisms occur simultaneously, but their kinetics are very different: in the first period, the structural rearrangement mechanism governs the aging of the amorphous alumina, whereas in the second period, Ostwald ripening controls the aging process. The combination of these two phenomena is the key to understanding the evolution of the specific surface area and pore volume. The structural rearrangement occurring during the first 5 min of the aging process liberates surface area and porosity within the texture of the particles. When the water loss proceeds more slowly, the steady growth of the crystallite size through Ostwald ripening leads to a continuous and significant decrease of the specific surface area. In this second period, the pore volume, which is much less sensitive to the crystallite size, decreases very slightly. It is interesting to note that Mullin et al.[10] similarly observed two periods in the aging of precipitated magnesium hydroxide. However, they obtain a continuous decrease of the specific surface area. Nevertheless, in their experimental investigation, the n values of eq 6 approached a value of approximately 3 only in the second period of aging, i.e., after 2 h, whereas during the first period, the values of n were significantly higher.

The pH of the aging medium has a considerable influence on the aging behavior of alumina gels. Marboe and Bentur[6] reported that aluminum hydroxide that had been precipitated at room temperature from a solution of 25 mL of (0.2 N) $Al(NO_3)_3$ and 25 mL of (1 N) NH_4OH and aged for 6 h in this alkaline medium (pH = 10) gave a well-defined bayerite X-ray pattern. However, a precipitate obtained from a mixture of 20 mL of (1 N) $Al(NO_3)_3$ and 10 mL of (1 N) NH_4OH and aged for 6 days in the acidic medium (pH = 5) maintained the amorphous X-ray pattern. The initial amorphous alumina in suspension maintained its amorphous X-ray pattern for several days. In contact with a solution having a pH higher than 7, gelatinous boehmite or pseudo-boehmite transforms into crystalline hydroxides. In the absence of alkali ions and in the presence of ammonia or amines, the transformation produces bayerite (or nordstrandite), whereas the conversion of bayerite to gibbsite occurs in the presence of alkali metal ions.[1] The rate of transformation increases with increasing pH and temperature. The transformation sequence can be represented by the scheme

$$Al^{3+} + 3OH^- \xrightarrow{pH = 8} \text{basic aluminum salt} \xrightarrow{pH = 8} \text{X-ray-amorphous gel} \xrightarrow{pH = 9} \text{pseudo-boehmite} \xrightarrow{pH > 10} \text{bayerite or nordstrandite} \xrightarrow{Na^+ \text{ or } K^+} \text{gibbsite}$$

A similar transformation sequence illustrates the relationships between the various alumina polymorphs and leads to crystalline boehmite. This transformation sequence is due to Lippens and Steggerda[19]

$$NaAl(OH)_4 + CO_2 \rightarrow \text{amorphous hydroxide} \xrightarrow{20\ ^\circ C,\ pH > 7} \text{gelatinous boehmite} \xrightarrow{20\ ^\circ C,\ pH > 9} \text{bayerite} \xrightarrow{20\ ^\circ C,\ pH > 12} \text{gibbsite} \xrightarrow{>80\ ^\circ C,\ pH > 12} \text{crystalline boehmite}$$

Previous experimental results[20] have shown that high salt concentrations delay, almost indefinitely, the conversion of pseudo-boehmite to bayerite. Generally, anions adsorbed on the solid retard the aging process. Wefers and Misra[2] reported the results of several authors on investigations of the interaction between anions and hydroxide gels. Gels precipitated in the presence of nitrate, sulfate, and carbonate ions behave as "positively charged polymeric materials". Whereas the interaction of nitrate appears to be predominantly electrostatic, sulfate and carbonate were found to coordinate with aluminum ions. Carbonate ion has the strongest retarding effect on the aging of alumina gels. The removal of acidic anions accelerates aging. Amorphous alumina gels (precipitated at pH's below 6 start-

ing from aluminum sulfate and sodium aluminate solutions) strongly retain sulfate ions. When precipitated at pH 9, these gels are crystalline.[4] Similarly, when comparing the effect of washing on alumina properties precipitated from nitrate solutions, Hellgardt and Chadwick[21] found that BET surface area, average pore size, and density are higher for aluminas with reduced nitrate contents. Hence, these results seem to indicate that crystallite size increases as the purity of the particles increases.

In the present work, where the aging times are no longer than 4 h, the polymorphic phase never exceeded the stage of pseudo-boehmite (see Figure 5). A mass balance of reagents used in the present experiments indicates that for 1 g L^{-1} of alumina produced, 1.14 g L^{-1} of Na_2SO_4 is obtained, which means that the prepared suspension has a high sulfate concentration. Earlier studies[6] indicate that aging and bayerite formation are delayed or prevented by the presence of sulfate ions. Our results are in agreement with the conclusions of Hsu[20] and Marboe and Bentur.[6] Sulfate ions can be considered to act as a chemical "glue", hindering, affecting, or suppressing dissolution. The formation of pseudo-boehmite involving only rearrangement is thus thermodynamically preferential. Such an interpretation was also made by Baltpurvins et al.[22] concerning the aging of ferrihydrite in the presence of sulfate ions. They observed that, in addition to its influence on the rate of transformation of ferrihydrite, the nature of the anions clearly affects the relative proportions and crystal morphologies of hematite and goethite in the final aged product. In the presence of sulfate ions, the formation of hematite is favored, and the average hematite crystal dimensions are increased. This phenomenon can be interpreted in terms of the competitive mechanisms of hematite and goethite formation. Goethite formation involves the dissolution of the ferrihydrite phase, followed by reprecipitation as goethite. Sulfate ions suppress the dissolution, so the formation of hematite, involving only rearrangement, is thus thermodynamically favored. Similarly, in this work, the high concentration of sulfate ions in the suspensions can be considered to act like a chemical glue, affecting the aging process and leading to pure pseudo-boehmite as the final aged product. Indeed, as can be seen from Figure 5, the aging process leads only to pseudo-boehmite particles; no traces of other polymorphs (bayerite, gibbsite, nordstrandite, etc.) are observed. These conclusions are also reinforced by a recent work[23] that clearly shows the central role of sulfate ions in the phase transformation of cobalt hydroxide from α to β form.

Modeling. For practical purposes, it is very interesting to identify, from the experimental data presented above, a relation expressing the rate constant A as a function of process parameters such as the temperature, pH, and salt concentration. Equations 3 and 4 show that A depends on D or k, $(\sigma/T)^p$, and $c_{eq}{}^p$, where the exponent p is equal to 1 or 2.

As a first approximation, the ratio σ/T does not depend on temperature.[24,25] In addition, Eble[26] gives a detailed physical model of the interfacial tension σ and shows that, in the case of alumina precipitation, it depends physically on the ionic strength, pH, and particle surface charge density.

The alumina solubility c_{eq} depends on temperature and pH. The functional expression can be obtained from the equilibrium scheme , which is valid for $T > 65$ °C and pH > 7[27]

$$Al(OH)_4^- + H^+ \leftrightarrow AlOOH\downarrow + 2H_2O$$

Thus, we have

$$[Al(OH)_4^-] = c_{eq} = \frac{K_b}{\gamma_{\pm}[H^+]} \tag{19}$$

where $\gamma_{\pm}$ is the activity coefficient.

The expression of K_b is

$$K_b = K_{b0} \exp\left(-\frac{E_{Kb}}{RT}\right) \tag{20}$$

with the following values for K_{b0} and E_{Kb}[27]

$$K_{b0} = 3.6 \times 10^{-4}\ \text{mol}^2/\text{L}^2 \quad \text{and} \quad E_{Kb} = 64\,800\ \text{J/mol}$$

Hence

$$c_{eq} \propto \frac{10^{pH}}{\gamma_{\pm}} \exp\left(-\frac{E_{Kb}}{RT}\right) \tag{21}$$

The molecular diffusion coefficient D and the kinetic constant k (k_1 or k_2) depend on temperature according to the Arrhenius laws $D = D_0 \exp(-E_D/RT)$ and $k = k_0 \exp(-E_k/RT)$. In addition, the frequency constant k_0 depends on the ionic strength.

As shown below, the dependence of A on the operating parameters is very complex. Nevertheless, we attempted to obtain a simple expression relating the influence of the temperature, ionic strength, and pH on the rate constant A. First, we noted from the experimental data that A is proportional to $10^{b\sqrt{I}}$. For this reason and on the basis of the above discussion, we propose a semiempirical relation of the form

$$A = 10^z \exp\left(-\frac{E}{RT}\right) \tag{22}$$

where $z = a + b\sqrt{I} + c \times$ pH; E is the overall activation energy of the aging process and a, b, and c are empirical constants. From eqs 3, 4, and, 21, we can deduce that $E = E_D + E_{Kb}$ or $E = E_k + pE_{Kb}$ (with p equal to 1 or 2). A regression analysis using all of the experimental data gives $a = 8.0$, $b = 0.6$, $c = 0.25$, and $E = 72\,300$ J mol^{-1}. Figure 11 shows good agreement between the experimental rate constant A and eq 22 (correlation index $r = 0.97$). Thus, using the E value obtained above, we can

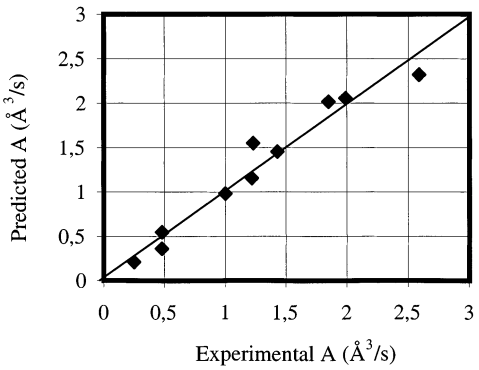

Figure 11. Parity plot for the volume growth rate coefficient.

deduce that E_k or E_D is equal to $E - pE_{Kb} = 72\,300 - 64\,800p$. From this result, it is clear that $p = 1$ and E_k or $E_D = 7500$ J mol^{-1}. Knowing that the activation energy values for diffusion and reaction are generally in the range $5 \times 10^3 < E_D < 1.5 \times 10^4$ J mol^{-1} and $4 \times 10^4 < E_k < 1.5 \times 10^5$ J mol^{-1}, it seems that the aging process of alumina in aqueous solutions is controlled by diffusion.

Conclusion

When amorphous alumina particles are abruptly transferred into an alkaline solution, an intensive ripening process occurs. The experiments performed in this work indicate that there are two mechanisms in the aging process, structural rearrangement and Ostwald ripening. The two mechanisms occur simultaneously, but their kinetics are very different. In the first period (i.e., the first 5 min of aging), the structural rearrangement mechanism is very rapid and governs the aging of alumina; the particles are transformed from an amorphous to a crystalline product, undergoing a dramatic water loss as shown by XRD and thermogravimetric analysis. In the second period, the structural rearrangement is almost finished, and Ostwald ripening controls the aging process.

Several authors have observed aging transformation sequences that ultimately led to polymorphs other than pseudo-boehmite. In this study, even under severe aging conditions ($T = 75$ °C, pH = 11.0, and aging time = 4 h), the final phase was always pseudo-boehmite. It is envisaged that the sulfate ions act as a chemical glue, suppressing dissolution of alumina particles and, hence, hindering particles from undergoing a polymorphic transformation. Sulfate ions seem to be a factor that can be adjusted to influence the rate of transformation.

It appears from the present study that the effects of pH, temperature, and ionic strength must be considered to provide the optimum conditions for the transformation of freshly precipitated amorphous alumina into pseudo-boehmite. In particular, despite its semiempirical character, eq 22 estimates well the influence of the above parameters, showing that the Ostwald ripening is controlled by diffusion. This equation can be used for practical purposes. For example, on the basis of the results obtained from eq 22, using continuous reactors, we have produced different kinds of alumina varying from anti-gastric pharmaceuticals to catalysts and catalyst supports.

Acknowledgment

The authors are grateful for the financial support from the European Commission through the BRITE-EURAM III Project. We express our special thanks to Hugues Dantigny of the Laboratoire de Sciences et Génie des Matériaux Métalliques for assistance in the TGA manipulations and to Dr. F. Villieras of the Ecole Nationale Supérieure de Géologie de Nancy for his interpretations regarding porosity.

Notation

$a(r)$, a_{eq} = activities of solute in equilibrium with crystals of size r and ∞, respectively, mol L^{-1}
b = width of the 111 peak of powdered silicium at half-maximum intensity, degrees
A, B = aging rate constants in eqs 5−10, Å^3 s^{-1}
C = measured width of the 021 peak of pseudo-boehmite at half-maximum intensity, degrees
C_{AS} = alumina suspension concentration, g L^{-1}
c_{eq} = solute equilibrium concentration (solubility), mol L^{-1}
E_D = diffusion activation energy, J mol^{-1}
E_k = reaction activation energy, J mol^{-1}
D = diffusion coefficient, m^2 s^{-1}
D_0 = constant in Arrhenius law for diffusion, m^2 s^{-1}
D_R = Rushton turbine diameter, m
H = height of liquid at the outlet pipe, m
h = height of Rushton turbine above reactor base, m
K_b = equilibrium constant, mol^2 L^{-2}
k_2 = kinetic constant of a second-order surface reaction, m^4 mol^{-1} s^{-1}
k_{20} = constant in Arrhenius law for reaction, m^4 mol^{-1} s^{-1}
M = molar weight, kg mol^{-1}
n = exponent in eq 6 depending on the ripening process
P/P_0 = relative adsorption measure in BET specific surface area determination
R = gas constant ($R = 8.314$), J mol^{-1} K^{-1}
$\bar{r}$ = mean characteristic crystal size, Å
t = time, s
t = statistical thickness of N_2 adsorbed on the surface of the particles at the relative pressure ratio P/P_0 used in t-plots, Å
T = absolute temperature, K
T_v = vessel diameter, m
$V_{0.98}$ = total N_2 volume adsorbed per gram of the sample of particles obtained at the relative adsorption pressure $P/P_0 = 0.98$ cm^3 g^{-1}
V_m = molar volume, m^3 mol^{-1}
V_p = total pore volume, cm^3 g^{-1}

Greek Letters

β = pure diffraction width, radians
$\gamma_\pm$ = mean ionic activity coefficient
$\bar{\epsilon}$ = mean power consumption, W kg^{-1}
θ = XRD diffraction angle, degrees
λ = XRD wavelength, Å
Λ = crystallite size, Å
ν_+, ν_- = numbers of cations and anions, respectively, in a molecular unit
ν = total number of ions ($= \nu_+ + \nu_-$)
ρ = particle density, kg m^{-3}
σ = interfacial tension, J m^{-2}
ϕ_s = area shape factor
ϕ_v = volume shape factor

Abbreviations

PSD = particle size distribution
XRD = X-ray diffraction

Symbol

■ = oxide vacancy for four- or five-coordinate AlO_x sites formed from six-coordinate sites

Literature Cited

(1) Misra, C., Ed. *Industrial Alumina Chemicals*; ACS Monograph 184; American Chemical Society: Washington, DC, 1986.

(2) Wefers, K.; Misra, C. *Oxides and Hydroxides of Aluminum*; Technical Paper No. 19; Aluminum Company of America: Pittsburgh, PA, 1987.

(3) Cocke, D. L.; Johnson, E. D.; Merrill, R. P. Planar Models for Alumina-Based Catalysts. *Catal. Rev. Sci. Eng.* **1984**, *26*, 163.

(4) Calvet, E.; Boivinet, P.; Noël, M.; Thibon, H.; Maillard, A.; Tertian, R. Contribution à l'Etude des Gels d'Alumine. *Bull. Soc. Chim. Fr.* **1953**, 99.

(5) Lippens, B. C. Structure and Texture of Aluminas. Ph.D. Dissertation, Uitgeverij Waltman-Delft, Delft, The Netherlands, 1961.

(6) Marboe, E. C.; Bentur, S. A New Interpretation of the Aging of Aluminum Hydroxide Gel. *Silic. Ind.* **1961**, *26*, 389.

(7) Nyvlt, J.; Söhnel, O.; Matuchova, M.; Broul, M. *The Kinetics of Industrial Crystallization*; Elsevier: Amsterdam, 1985.

(8) Kahlweit, M. Ostwald Ripening of Precipitates. *Adv. Colloid Interface Sci.* **1975**, *5*, 1.

(9) Hanitzch, E.; Kahlweit, M. Aging of Precipitates. In *Industrial Crystallization Symposium*; Institution of Chemical Engineers: London, 1969; p 130.

(10) Mullin, J. W.; Murphy, J. D.; Söhnel, O.; Spoors, G. Aging of Precipitated Magnesium Hydroxide. *Ind. Chem. Eng. Res.* **1989**, *28*, 1725.

(11) Gruy, F.; Cournil, M. A New Approach to Ostwald Ripening: Behaviour at Early Stages and Influence of the Grain Connectivity. In *Proceedings of the 13th Symposium on Industrial Crystallization*; Institution of Chemical Engineers: London, 1996; Vol. 2, p 803.

(12) Villieras, F. Ecole des Mines de Nancy, Nancy, France. Personal communication, 1999.

(13) Klug, H. P.; Alexander, L. E. *X-ray Diffraction Procedures*, 2nd ed.; John Wiley & Sons: New York, 1974.

(14) Johnson, M. F. L.; Mooi, J. The Origin and Type of Pores in Alumina Catalysts. *J. Catal.* **1968**, *10*, 342.

(15) Ono, T.; Oghuchi, Y. Control of the Pore Structure of Porous Alumina. In *Preparation of Catalysts III*; Poncelet, G., Grange, P., Jacobs, P. A., Eds.; Elsevier Science Publishers: Amsterdam, 1983.

(16) Baker, B.; Pearson, R. M. Pseudo-Boehmite Water Content and Structure. *J. Catal.* **1974**, *33*, 265.

(17) Papée, P.; Tertian, R.; Biais, R. Recherches sur la Constitution des Gels et Hydrates Cristallisés d'Alumine. *Bull. Soc. Chim. Fr.* **1958**, *10*, 1301.

(18) Fitzgerald, J. J.; Piedra, G.; Dec, S. F.; Seger, M.; Maciel, G. E. Dehydration Studies of a High-Surface-Area Alumina (Pseudo-Boehmite) Using Solid State ^{1}H and ^{27}Al NMR. *J. Am. Chem. Soc.* **1997**, *119*, 7832.

(19) Lippens, B. C.; Steggerda, J. J. *Physical and Chemical Aspects of Adsorbents and Catalysts*; Academic Press: London, 1970.

(20) Hsu, P. H. Effects of Salts on the Formation of Bayerite versus Pseudoboehmite. *Soil Sci.* **1967**, *103*, 101.

(21) Hellgardt, K.; Chadwick, D. Effect of pH of Precipitation on the Preparation of High Surface Aluminas from Nitrate Solutions. *Ind. Eng. Chem. Res.* **1998**, *37*, 405.

(22) Baltpurvins, K. A.; Burns, R. C.; Lawrance, G. A.; Stuart, A. D. Effect of pH and Anion Type on the Aging of Freshly Precipitated Iron (III) Hydroxide Sludges. *Environ. Sci. Technol.* **1996**, *30*, 939.

(23) Lim, W. L. Etude cinétique et caractérisation de produits d'une precipitation avec transformation de phase: Application à la synthèse de l'hydroxyde de cobalt(II)β. Ph.D. Dissertation, Ecole Nationale Supérieure des Mines de Paris, Paris, France, 2000.

(24) Söhnel, O.; Garside J. *Precipitation: Basic Principles and Industrial Applications*; Butterworth-Heinemann: London, 1992.

(25) Mersmann, A. Calculation of Interfacial Tensions. *J. Cryst. Growth* **1990**, *102*, 841.

(26) Eble, A. Precipitation of Nanoscale Crystals with Particular Reference to Interfacial Energy. Ph.D. Dissertation, Technischen Universität München, München, Germany, 2000.

(27) Rousseaux, J. M. Conception, mise en oeuvre et modélisation de réacteurs pour la precipitation de particules à propriétés contrôlées. Application à la pseudo-boehmite. Ph.D. Dissertation, Institut National Polytechnique de Lorraine, Nancy, France, 2000.

Received for review January 12, 2000
Revised manuscript received February 23, 2002
Accepted July 28, 2002

IE000053P